

3D Printing of Strong and Tough Double Network Granular Hydrogels

Matteo Hirsch, Alvaro Charlet, and Esther Amstad*

Many soft natural tissues display a fascinating set of mechanical properties that remains unmatched by manmade counterparts. These unprecedented mechanical properties are achieved through an intricate interplay between the structure and locally varying the composition of these natural tissues. This level of control cannot be achieved in soft synthetic materials. To address this shortcoming, a novel 3D printing approach to fabricate strong and tough soft materials is introduced, namely double network granular hydrogels (DNGHs) made from compartmentalized reagents. This is achieved with an ink composed of microgels that are swollen in a monomer-containing solution; after the ink is additive manufactured, these monomers are converted into a percolating network, resulting in a DNGH. These DNGHs are sufficiently stiff to repetitively support tensile loads up to 1.3 MPa. Moreover, they are more than an order of magnitude tougher than each of the pure polymeric networks they are made from. It is demonstrated that this ink enables printing macroscopic, strong, and tough objects, which can optionally be rendered responsive, with high shape fidelity. The modular and robust fabrication of DNGHs opens up new possibilities to design adaptive, strong, and tough hydrogels that have the potential to advance, for example, soft robotic applications.

non-covalent interactions,^[10,11] slide-ring structures,^[12] host-guest interactions,^[13] nanoparticle fillers,^[14] or a combination of them^[15] are introduced. Indeed, this strategy enables the design of extremely tough hydrogels that can be stretched up to 50 times.^[16–18] However, these tough hydrogels are typically rather soft such that they cannot bear significant loads under tension. To overcome this shortcoming, double network (DN) hydrogels composed of two interpenetrating polymeric networks have been introduced. These DN hydrogels are composed of a highly cross-linked network, the filler, that imparts stiffness to the hydrogel and a second loosely cross-linked one, the matrix, that imparts toughness to it.^[19] This advance enabled engineering the mechanical properties of DN hydrogels to be similar to those of certain natural tissues such as cartilage.^[20,21]


Despite a great improvement in mechanics, manmade hydrogels are typically inert and hence, cannot adapt their

1. Introduction

Hydrogels are often used for moisturizing purposes, for example in wound healing,^[1] drug delivery,^[2] or food^[3] owing to their ability to retain large amounts of water, intrinsic biocompatibility, and the possibility to be functionalized with various moieties. In addition, hydrogels possess the ability to retain a 3D structure and to support cell growth rendering them well-suited replacements for soft biological tissues,^[4–6] and for soft robotics.^[7–9] Most hydrogels that must retain their 3D structure and bear some load are covalently cross-linked and hence, if swollen, they are inherently brittle. Their toughness can be strongly increased, if reversible crosslinks that rely on

properties in response to external stimuli, in stark contrast to many natural counterparts. An important difference between these two types of materials is their structure and local composition. Soft natural materials possess locally varying compositions and structures that are well-defined over many length scales. By contrast, synthetic hydrogels typically have an ill-defined microstructure and their composition is most often homogeneous. Variations in the composition can be introduced using magnetic nanoparticle gradients,^[22] ultraviolet (UV) patterning,^[23] micro-molding,^[24] photo-triggered chemical cross-linkers,^[18] or micro-phase separation.^[25] Another remarkable example of controlling the microstructure of soft synthetic materials is the incorporation of liquid crystals into polymer chains. This was nicely shown on liquid crystal elastomers.^[26–29] However, these methods are often labor intense such that they cannot fabricate soft materials with structures that are similar to those of natural models. A contributing reason for the discrepancy in the structure and local composition of soft natural versus synthetic materials is the difference in their processing. Nature produces many of its strong and tough materials from compartmentalized reagents. For example, most marine mussels fabricate their byssus from precursor-containing vesicles that are released on demand and self-assemble into well-defined structures.^[30,31] By contrast, synthetic hydrogels are typically fabricated by mixing reagents in bulk. This technique offers an excellent control over the overall composition of the hydrogels. However, it lacks control over the local composition

M. Hirsch, A. Charlet, Prof. E. Amstad
Soft Materials Laboratory
Institute of Materials
École Polytechnique Fédérale de Lausanne
Lausanne CH-1015, Switzerland
E-mail: esther.amstad@epfl.ch

 The ORCID identification number(s) for the author(s) of this article can be found under <https://doi.org/10.1002/adfm.202005929>.

© 2020 The Authors. Advanced Functional Materials published by Wiley-VCH GmbH. This is an open access article under the terms of the Creative Commons Attribution License, which permits use, distribution and reproduction in any medium, provided the original work is properly cited.

DOI: 10.1002/adfm.202005929

and microstructure. Inspired by nature, we fabricated hydrogels composed of hexagonal prismatic microgels with well-defined microstructures and locally varying compositions.^[32] However, this technique is limited to the fabrication of thin sheets. More complex 3D structures can be achieved through patterned droplet networks^[33] or jammed microgels, for example, using additive manufacturing techniques.^[34–37] However, monodisperse spherical microgels have a small contact area such that the resulting superstructures are weak.^[38] The mechanical properties of these granular materials can be improved if the surfaces of the microgels are modified with thiols^[39] or metal-coordinating groups,^[40] through covalent crosslinking of adjacent microgels,^[41] or by means of a percolating second network.^[42,43] However, the increased adhesion between microgels compromises the stretchability of the materials, thereby reducing their toughness. Methods to fabricate strong and tough complex 3D hydrogels that have the potential to be used, for example, as load-bearing parts of soft robots, remain to be established.

Here, we introduce a new ink that can be additive manufactured into strong and tough double network granular hydrogels (DNGHs) with locally varying compositions. The ink is composed of polyelectrolyte-based microgels that are swollen in a monomer-loaded solution. This monomer-loaded solution can be converted into a percolating network after the ink has been processed into macroscopic materials. The new two-step approach separates the fabrication of microgels and their annealing. Thereby, it combines the advantages of jammed

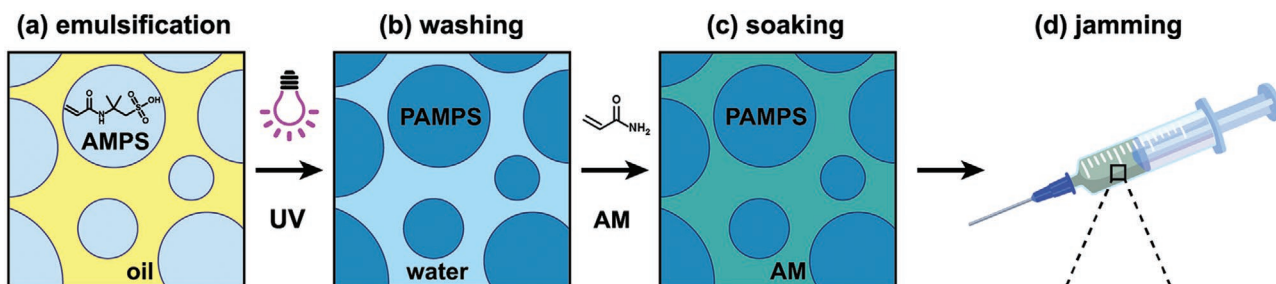
granular solutions such as injectability and printability with the excellent mechanical properties of DN hydrogels. Importantly, the mechanical properties of the additive manufactured materials can be tuned with the composition of the ink and are independent of the printing parameters such as the printing direction. Because this new technology employs a microgel-based ink, it significantly extends the choice of materials that can be additive manufactured such that the range of mechanical properties that can be accessed with 3D printed hydrogels is much wider. Our new DNGHs promise to bridge the gap between structural complexity and mechanical performance that plays a key role in the advancement of soft materials for load-bearing applications. These features will likely enable the design of new, functional, and responsive hydrogels that can be used for soft robots and actuators, and membranes for wastewater treatment.

2. Results and Discussion

2.1. Microgel Ink Design and Fabrication

To maximize the contact area between adjacent microgels and minimize interstitial spaces, we synthesize microgels possessing a high swelling capacity. Polyelectrolyte-based microgels have been shown to fulfill these requirements. Hence, we select 2-acrylamido-2-methylpropane sulfonic acid (AMPS) as a model system and fabricate AMPS microgels from reagent-loaded

Microgel ink preparation



DNGH 3D printing and post-curing

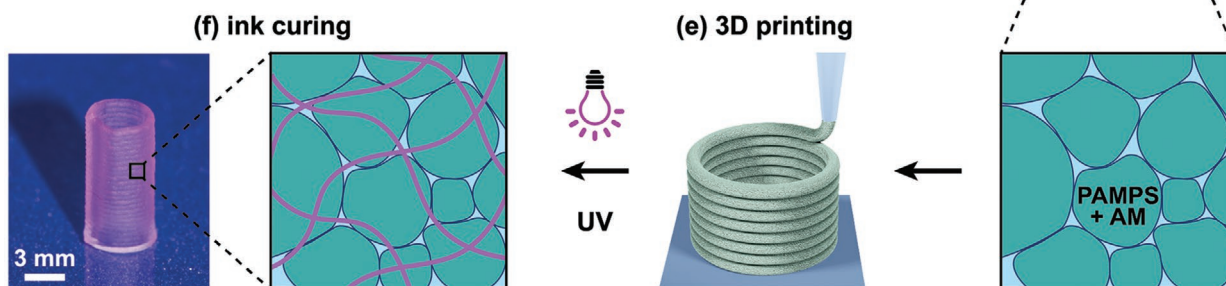


Figure 1. Additive manufacturing of DNGHs. Schematic representation of microgel fabrication. a) A monomer-containing aqueous solution is processed into a water-in-oil emulsion. b) AMPS-loaded drops are converted to PAMPS microgels through a UV-induced polymerization. c) Microgels are soaked in an AM monomer-containing solution. d) Monomer-loaded microgels are jammed to yield a printable ink. e) Jammed microgels are extruded as a continuous filament that displays fast shear recovery, enabling the printing of granular hydrogels possessing high aspect ratios with a high shape fidelity. f) The 3D printed objects are post-cured through an exposure to UV light that initiates the polymerization of the AM monomers to form a percolating network, as exemplified by the 3D printed cylinder.

water-in-oil emulsion drops, as sketched in **Figure 1(i)** and detailed in the Experimental Section. To test if the size of the microgels we produce scales with that of the emulsion drops, we quantify this parameter from optical microscopy images. Drops and cross-linked microgels are nearly identical in size, as shown in **Figure S1**, Supporting Information. After having been cross-linked, microgels are washed several times in ethanol and deionized water to remove any unreacted molecule, as sketched in **Figure 1(ii)**. To ensure good inter-particle adhesion, which plays a key role for obtaining good mechanical properties, we swell the microgels in a solution containing reagents that can be converted into a percolating network after the microgels have been 3D printed. Here, we swell the microgels in an aqueous solution containing acrylamide (AM) monomers, as sketched in **Figure 1(iii)**. To avoid any dilution effects from the water exchange, we soak microgels in the monomer solution for 24 h in large excess of the second network precursor solution. The degree of swelling of the microgels strongly depends on the cross-linker concentration of the microgels: microgels containing 14 mol% cross-linker have an average diameter of 40 μm whereas those containing 3.5 mol% cross-linker have a diameter of 120 μm , as shown in **Figure S1**, Supporting Information.

An important feature of our technique is the processing of individually dispersed microgels into macroscopic materials with structures that are well-defined over the millimeter up to the centimeter-length scales. To enable 3D printing of the dispersed microgels, we jam them using vacuum filtration, as shown in **Figure 1(iv)**. The resulting ink is additive manufactured into complex structures, as schematically presented in **Figure 1(v)**. The printed construct is then post-cured by exposing it to UV light to allow the formation of a percolating second network, as exemplified on **Figure 1(vi)**.

2.2. Rheological Characterization of Microgel Inks

A prerequisite for inks to be 3D printed into macroscopic complex structures is their shear-thinning behavior, which is a common property of bioinks^[44,45] and jammed microgels.^[46] To ensure a reproducible jamming of the microgels, we measure the solid polymer content of samples swollen in deionized water, as reported in **Table S1**, Supporting Information. The results suggest a good reproducibility of our jamming process, where the AMPS polymer content accounts for 4.83 wt% of the resulting ink. The standard deviation of the solid fraction is as low as 0.22 wt%.

As expected, our jammed microgels are shear-thinning, as demonstrated by oscillatory rheology in **Figure 2a**. The viscosity of the jammed PAMPS microgels can be tailored with the cross-linker concentration; it increases from 100 to 1000 Pa·s at a shear rate of 10 s^{-1} , if the cross-linker concentration is increased from 3.5 to 14 mol%. To enable precise dosing, the solid granular ink should possess a low flow point. This requirement is fulfilled by our jammed PAMPS microgels, as shown in **Figure 2b**. Indeed, the flow point is in the range of 10% for all the different formulations. Furthermore, we observe no influence of the monomer loading on the flow point of our granular ink, as shown in **Figure S2**, Supporting Information.

To obtain a good printing resolution, the ink must rapidly solidify after it has been extruded, which is the case if it displays fast stress healing properties. Indeed, our jammed PAMPS solution recovers almost immediately and repetitively from a liquid-like state at high strains, to a viscoelastic state at low strains, as shown in **Figure 2c**. To test if this behavior is temperature-dependent, we perform step strain relaxation measurements at temperatures varying between 5 and 45 °C. The relaxation time of our jammed microgels remains the same between 5 and 45 °C, as shown in **Figure S3a**, Supporting Information, such that these microgels can be easily processed within this temperature range. This behavior is inherent to jammed microgels that behave as solid-like materials because their linear elasticity is governed by the microgel composition.^[46] Hence; our results indicate that the jammed microgels possess rheological properties that are well-suited for additive manufacturing.

Jammed microgels can form macroscopic, porous materials that retain their structure.^[34,37,41] However, the lack of covalent adhesion between particles makes them mechanically weak such that they cannot bear significant loads. To overcome this shortcoming, we transform jammed microgels into a mechanically robust material by forming a second percolating network within the jammed microgels. This is achieved by exposing the granular construct to UV light to initiate the polymerization of the AM monomers. To follow the gelation kinetics of the percolating second network, we perform time-dependent oscillatory rheology measurements. Results suggest that gelation plateaus around 150 s, as shown in **Figure S3b**, Supporting Information. As a result of the formed percolating PAM network, the DNGH retains its integrity, in stark contrast to jammed microgels that relax stress over time, as shown in **Figure 2d**.

2.3. Mechanical Characterization of DNGHs

The mechanical properties of hydrogels are strongly influenced by the weight fraction of the polymers. To characterize the polymer fraction of our DNGHs, we compare the weight of DNGHs as prepared and that of dried DNGHs as a function of their composition. Depending on the composition of our DNGHs, their dry polymer content ranges from 13.6 to 45.7 wt%, as summarized in **Figure S4a**, Supporting Information. To predict their swelling behavior, we compare the dry polymer content with the equilibrium water content (EWC) of our DNGHs. EWCs range from 81.5 to 98.0 wt% depending on DNGH composition, as summarized in **Figure S4b**, Supporting Information.

Granular hydrogels inherently possess locally varying compositions. In our case, grains are composed of PAMPS that are reinforced by PAM and hence, they constitute DN hydrogels. By contrast, the grain boundaries are composed of PAM only. To test the influence of the composition of our hydrogels on their mechanical properties under tension, we perform tensile tests on as-prepared DNGHs composed of AMPS microgels fabricated from a 30 wt% monomer solution and a second network made from a solution containing 20 wt% AM. The granular hydrogel is significantly stiffer and tougher than bulk hydrogels composed of either PAMPS or PAM. The Young's modulus of

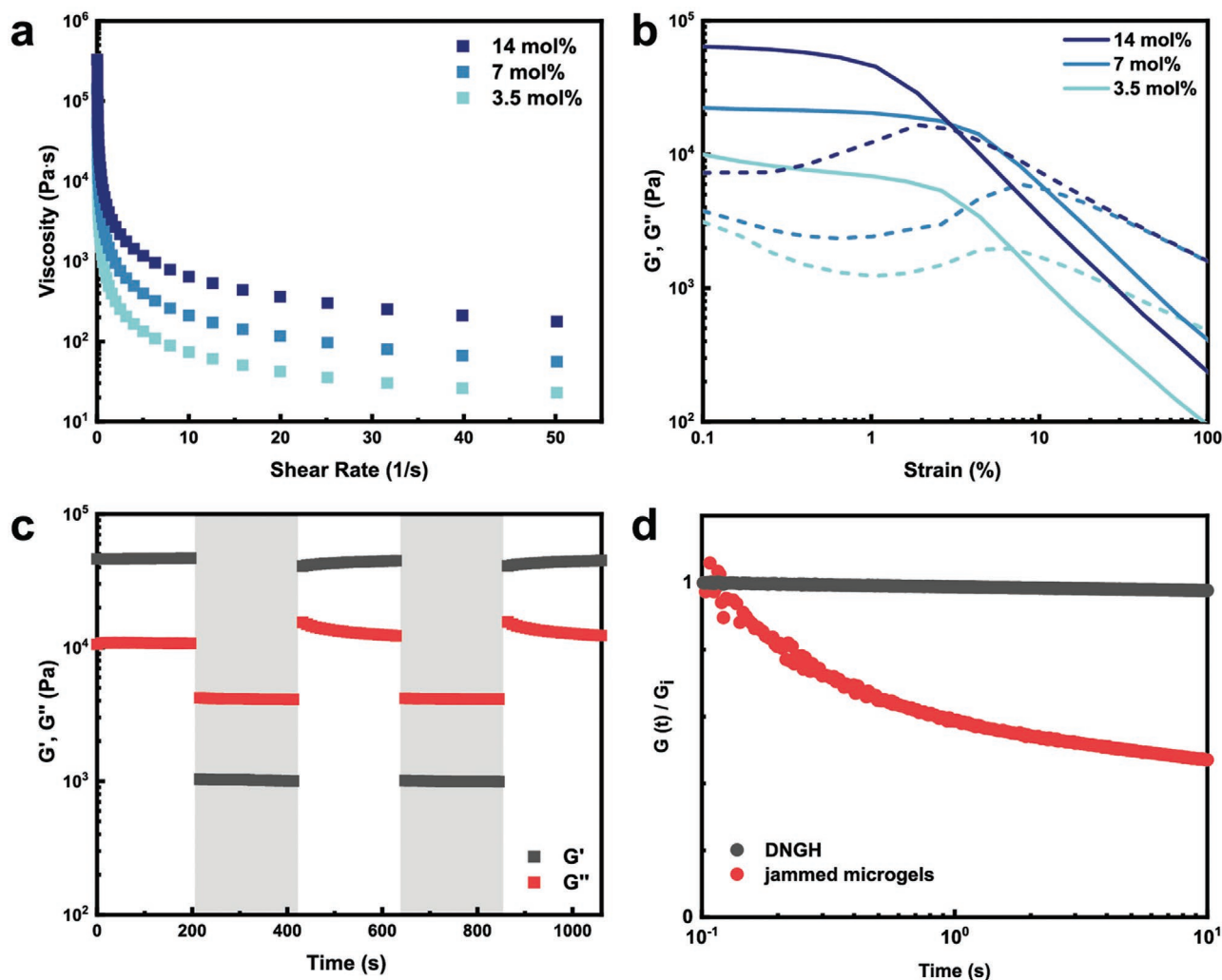


Figure 2. Rheology of jammed microgels. a,b) Frequency dependent viscosity (a) and amplitude sweep (b) of jammed microgels containing different cross-linker concentrations. All three samples display a characteristic shear-thinning behavior and a low yield strain. c) Self-healing behavior of jammed microgels containing 3.5 mol% cross-linker. The material transitions from a solid-like to a liquid-like state when subjected to high shear ($\gamma = 30\%$). The jammed solution recovers rapidly to its initial condition at low shear ($\gamma = 1\%$). The process can be repeated cyclically without deterioration of the ink performance. d) Step strain relaxation of a DNGH and jammed microgel ink. The difference in relaxation time is due to the presence of the second percolating network in DNGH.

the DNGH is fivefold higher than that of PAMPS and threefold higher than that of PAM. We attribute the high stiffness of DNGH to the chain entanglements that are topologically constrained between PAM chains and the microgel network, such that they cannot be easily displaced.^[47] However, our DNGHs are twofold softer than unstructured DN counterparts, as summarized in **Figure 3a**. We assign this difference to the PAMPS network that is not percolating the entire DNGHs but is only present within the microgels, in stark contrast to DNs.

A key requirement for the use of hydrogels for load-bearing applications is that they are tough such that they do not fail catastrophically if deformed within a well-defined range. To assess the toughness of our DNGHs, we quantify their fracture strength. The fracture strength of the DNGH is more than tenfold higher than that of bulk PAMPS and PAM. Remarkably, the fracture strength of DNGHs is even threefold higher than that of the unstructured DN counterparts, despite of its

lower Young's modulus, as shown in **Figure 3a**. We attribute the corresponding increase in toughness to a stress concentration at the poles of the microgels due to a substantial mismatch in elasticity of the two interpenetrating networks, as has been described for microgel reinforced hydrogels.^[48] These results demonstrate the potential of granular hydrogels possessing locally varying compositions for load-bearing applications and as dampers.

Most soft natural materials are subjected to complex loading profiles.^[6] To test if our DNGH is sufficiently robust to sustain more demanding loading profiles, we perform compression measurements on DNGH, PAMPS, and PAM samples. The compressive modulus of the DNGH is twofold higher than that of PAM, as shown in **Figure S5a**, Supporting Information. The compressive stress increases even more: it reaches 0.8 MPa at 60% strain which is three times higher than that of the PAM network. Furthermore, we test its ability to lift a 1 kg weight

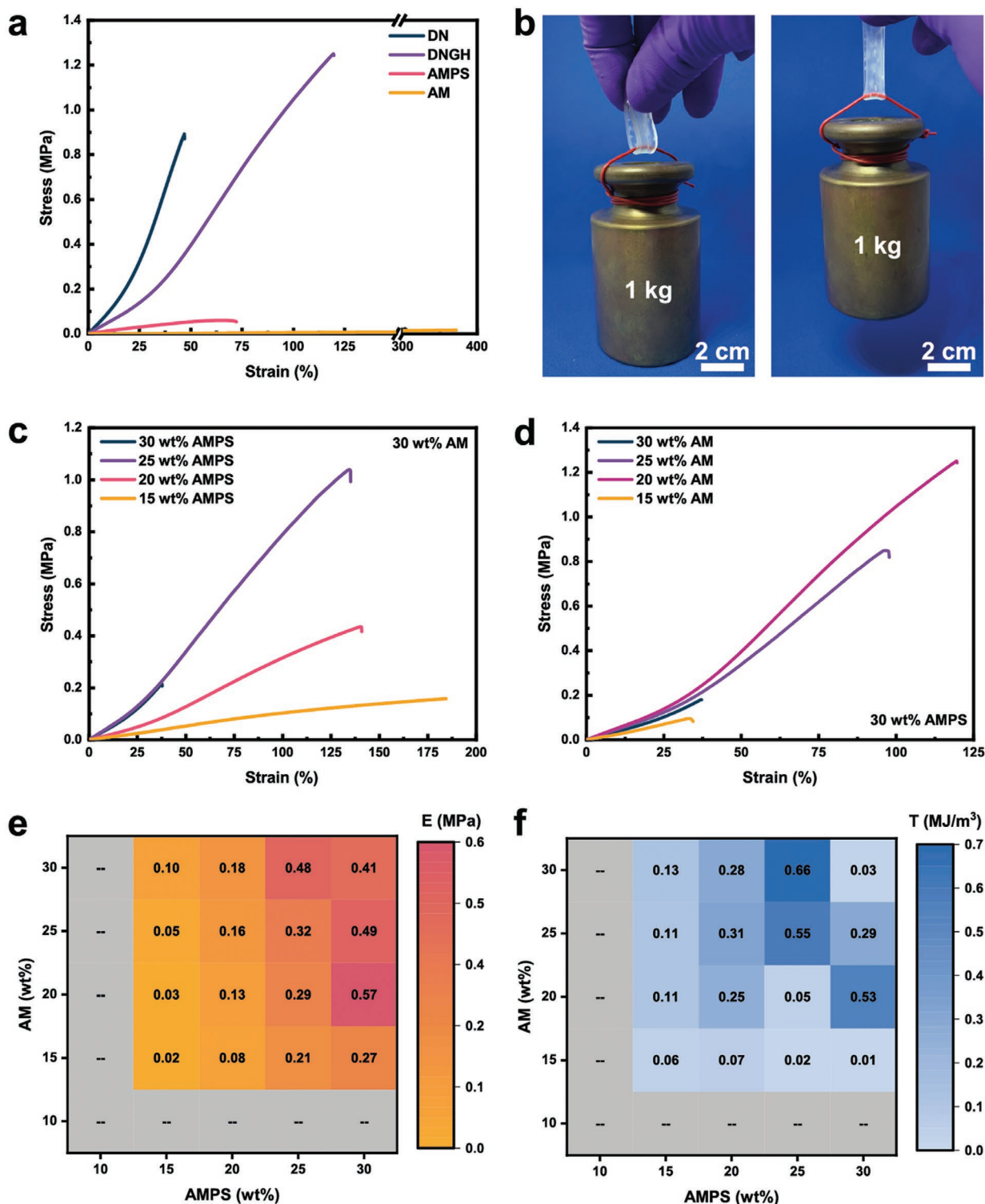


Figure 3. Mechanical characterization of DNGHs. a) Tensile tests of DNGH are compared to those of bulk PAMPS-PAM DN, and single PAM and PAMPS hydrogels. The granular material displays a toughening behavior typical of DN hydrogels that is threefold higher than the bulk DN counterpart. b) Photograph of a hydrogel stripe with a cross section of $10 \times 2 \text{ mm}^2$ that has been loaded with a 1 kg weight. c) Tensile measurements of DNGHs prepared with 30 wt% AMPS microgels and a PAM second network made from varying AM concentrations. The toughness of the samples increases with increasing AM concentration until it peaks at 25 wt% AM. d) Tensile measurements of DNGHs made of PAMPS microgels synthesized with varying AMPS concentrations that are embedded in a percolating network made from 30 wt% AM. The elasticity of the DNGHs increases with increasing AMPS concentration. e,f) Color maps of the Young's moduli (e) and toughness (f) calculated as the area under the stress–strain curve of DNGHs as a function of the concentration of AMPS contained in the microgels and that of AM that forms the second percolating network. Reported values represent the mean of five repeated measurements.

through a folded rectangular stripe with a cross section of 10 mm × 2 mm, as shown in Figure 3b. Remarkably, the stripe is able to support the applied load for at least five loading cycles with no appreciable weakening, as exemplified in Movie S1, Supporting Information. These results demonstrate the potential of our DNGHs to be used for load-bearing applications.

The elasticity of DN hydrogels depends on the initial polymer content and cross-linker concentration of the first network.^[19] To test if this is also the case for our DNGH where the first network is not percolating, we fabricate microgels containing different polymer contents and perform tensile tests on them. Indeed, the Young's modulus of the DNGH increases from 0.10 to 0.48 MPa with increasing polymer content until it reaches a plateau at 25 wt% AMPS, as shown in Figure 3c. The lower mechanical performance of the DNGH at 30 wt% AMPS is related to the poor swelling of the microgels in the second AM solution. A similar behavior is observed if we fix the polymer content of the AMPS microgels and vary the cross-linker concentrations. For example, DNGHs prepared with 14 mol% *N,N'*-methylene bisacrylamide (MBA) cross-linker possess a Young's modulus fourfold higher than the corresponding sample containing only 3.5 mol% MBA, as shown in Figure S5b, Supporting Information. However, the increase in the microgel cross-linker density decreases the fracture strain of the DNGH from 150% to 65%. To ensure good elasticity of the printed construct while maintaining good mechanical integrity, we keep the crosslink density of the microgels constant at 3.5 mol% in the following experiments.

Our results indicate that the mechanical properties of our DNGHs strongly depend on the polymer content of the microgels and the second percolating network. To determine the best combination of the polymer contents of the microgels and the percolating network, we systematically and independently vary these two parameters and quantify the Young's modulus and toughness of the resulting materials from tensile tests. The Young's modulus of our DNGHs increases with increasing AMPS concentration, independent of the AM concentration used to form the second percolating network, as summarized in Figure 3e. This finding is in agreement with unstructured DN where the elasticity is mainly determined by the first network.^[21,49] The Young's modulus of our DNGHs can reach values up to 0.57 MPa if they are composed of 30 wt% AMPS and 20 wt% AM.

The toughness of unstructured DNs is mainly determined by the loosely cross-linked secondary network.^[16,44] To test if this is also the case for our DNGHs, we quantify the toughness, calculated as the area under the stress–strain curve, for all the tested samples. Indeed, the toughness of our DNGHs increases with increasing AM concentration, as summarized in Figure 3d. The one clear exception to this trend presents the stiffest DNGHs that we formed, that also display a high toughness of 0.53 MJ m⁻³. The maximum toughness of 0.66 MJ m⁻³ is achieved for DNGHs prepared with 25% AMPS and 30% AM, as summarized in the color map in Figure 3f. The color maps of the Young's modulus and toughness of our DNGHs nicely show that their mechanical properties can be tuned over a wide range by adjusting the concentrations of monomers used to form the microgels and the secondary network, respectively.

An additional parameter that strongly influences the mechanical properties of unstructured DNs is the cross-linker density of the second network. To test if this is also the case for our DNGHs, we fabricate DNGHs with two different AM cross-linker densities and test them under tension. At 0.02 mol% cross-linker concentration, the material displays the yielding behavior that is characteristic for conventional DN hydrogels, as shown in Figure S6a, Supporting Information. However, because of the low crosslink density, the bonds between microgels are weak such that the material easily ruptures along the grain boundaries, as shown in Figure S6b, Supporting Information. These results suggest a weak inter-particle adhesion. The toughness strongly increases, if we increase the AM crosslink density; by increasing it tenfold, the fracture strength increases from 50 to 600 kPa. Importantly, the increase in toughness does not compromise the stiffness of the DNGH; the Young's modulus remains unchanged at 0.28 MPa. As a consequence, the fracture toughness of the DNGH increases more than tenfold if we increase the AM concentration to 0.2 mol%. These results demonstrate that the mechanical properties of DNGH can be tuned with the crosslink density of the percolating network, by analogy to DN materials that contain individually dispersed microgels in them.^[47] However, by contrast to the DN materials, our DNGH can be additive manufactured into complex shapes. To ensure good shape-retaining properties of the ink and a good stability of the additive manufactured materials, we employ the formulation containing 0.2 mol% cross-linker for the following experiments.

2.4. Printability and Post-Curing Stability of DNGHs

An important asset of our DNGH is their fabrication from jammed microgels that shear-thin and rapidly recover when stress is relieved. We expect this rheological behavior to render our jammed microgels well-suited inks for 3D printing. When the ink is extruded through a 410 μm diameter nozzle, it is subjected to significant shear stresses that lower the viscosity of the ink locally. The fast recovery of the elastic properties upon relaxation of the stress allows extruding a stable filament whose diameter is similar to that of the nozzle, as shown in the photograph in Figure 4a. Importantly, the extruded filament maintains the characteristic granularity of the ink, as evidenced from the fluorescent micrograph in Figure 4b.

Macroscopic 3D structures are typically printed by depositing multiple layers on top of each other. To ensure good integrity of the 3D printed structures, subsequent layers must partially merge. Our ink is fundamentally different in that it is composed of jammed microgels that can re-arrange before a second percolating network is formed such that we expect it to enable printing junctions with good interconnections. To test our expectation, we print two perpendicular filaments in a grid-like geometry, as shown in Movie S2, Supporting Information. Indeed, the junctions display good interconnectivity between adjacent layers already before the second percolating network is formed, as shown in Figure 4c. After the second percolating network is formed, the grid retains its shape and integrity even if removed from the substrate, as shown in Figure 4d.

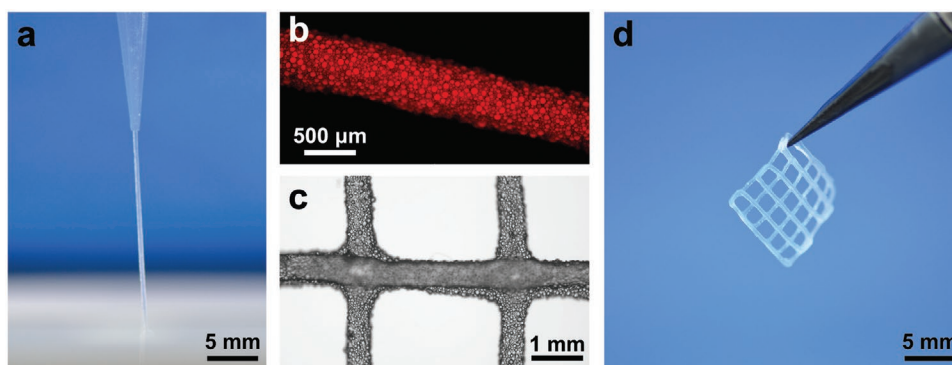


Figure 4. Printing of jammed microgels. a) Photograph of the jammed microgel filament while it is extruded from a 410 μm conical nozzle. The material can be printed continuously without rupture yielding a filament with high shape fidelity. b) Fluorescent micrograph of the extruded granular filament. Microgels are labeled with sulforhodamine B sodium salt. The resulting granular filament has an average diameter of 500 μm . c) Optical micrograph of a printed grid demonstrating the high shape-retaining properties of the extruded layers. The curvature between crossing filaments suggests partial merging of subsequent layers. d) Photograph of a free-standing DNGH grid. Upon UV curing, the printed object can be removed from the substrate while retaining its shape, demonstrating the good interconnectivity between layers that is caused by the percolating second PAM network.

The mechanical properties of additive manufactured materials are typically inferior to those of the corresponding bulk materials. This discrepancy is often related to a weak adhesion between sequentially deposited layers. Our ink offers an elegant possibility to overcome this limitation as the second, percolating network is formed after the ink is 3D printed. Therefore, we expect the interfaces between sequentially deposited layers to be equally strong as the grain boundaries within the printing plane. To test this hypothesis, we print a solid DNGH rectangular stripe where the printing direction is along its length and one where the printing direction is perpendicular to it, as schematically shown in **Figure 5a**. Remarkably, we do not observe any significant influence of the printing direction on the mechanical properties of these stripes, as shown in **Figure 5b**. This is in stark contrast to polymers that are additive manufactured using conventional, homogeneous inks.^[50] Indeed, the Young's modulus is the same as the one measured for molded samples, 0.28 MPa. Interestingly, the additive manufactured samples possess a higher toughness than the corresponding molded ones: DNGH printed stripes reach a fracture

strength of more than 0.8 MPa and a maximum elongation of around 290%, compared to the molded samples whose fracture strength is 0.6 MPa and the maximum elongation is 150%. The superior mechanical properties are likely related to the more homogeneous distribution of microgels in printed samples and the lower density of defects such as air inclusions.

To put the mechanical performance of our 3D printed DNGHs in perspective with previously reported 3D printed hydrogel, we compare the Young's moduli of these systems. Our DNGHs are stiffer than any of the previously reported formulation, as summarized in **Figure 6**.^[39,51–58] We assign this difference to the processing: our DNGHs are fabricated from jammed microgels such that we can independently optimize the rheological properties of the ink and the composition of the microgels. This is in stark contrast to most 3D printed hydrogels where these two parameters are closely coupled. Taking advantage of this important aspect, we can combine the extraordinary mechanical properties of DN hydrogels with an additive manufacturing process, without compromising the printability and resolution of the ink.

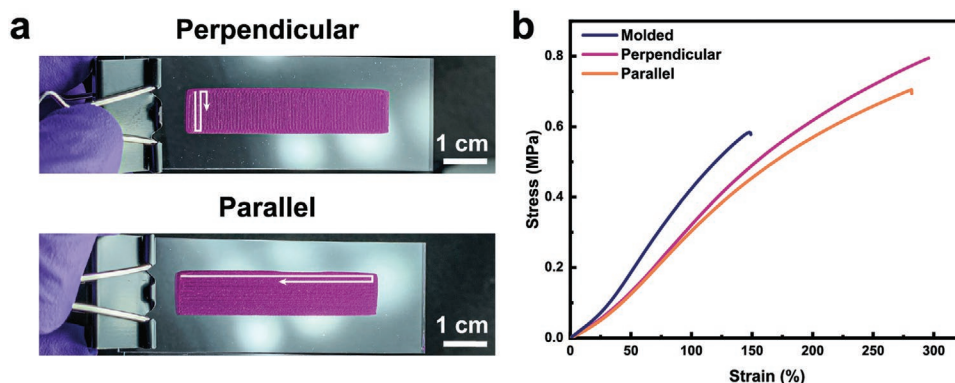


Figure 5. Effect of printing direction on mechanical properties. a) Photograph of DNGH stripes printed with perpendicular (top) or parallel (bottom) filament orientation. Microgels are labeled with sulforhodamine B sodium salt for visualization. b) Tensile measurements of DNGH stripes printed parallel and perpendicular to the long axis of the stripe. We cannot observe any influence of the printing direction on the mechanical properties. The toughness of additive manufactured DNGHs is significantly higher than that of molded samples.

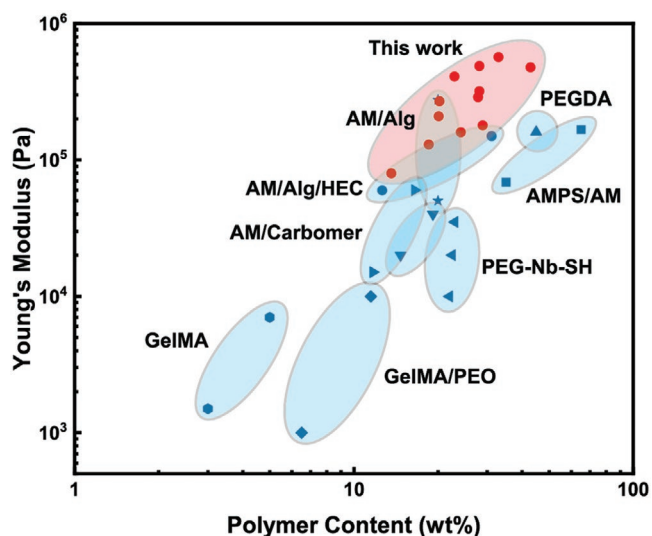


Figure 6. Ashby plot. Young's moduli of various hydrogel inks plotted as a function of the total polymer content. DNGHs reported in this paper are stiffer than any other previously reported 3D printed hydrogel.

2.5. Potential Applications of DNGHs

Our results suggest that jammed microgels soaked in a monomer solution are well-suited inks to additive manufacture strong and tough 3D hydrogels. This is an asset that has been difficult to achieve with previously reported 3D printed hydrogels.^[59–61] To exploit this new feature, we 3D print our jammed microgels into high aspect ratio hollow cylinders, as shown in Figure 7a. Indeed, the additive manufactured DNGH structure can be repetitively compressed up to 80%, where it buckles, and retains its initial shape when the stress is released, as shown in Movie S3, Supporting Information. Importantly, we do not observe any signs of damage, even after samples have been unloaded, as shown in Figure 7b. The exceptional shape fidelity and mechanical stability of the construct hints at the potential of the jammed microgel-based ink to design mechanically robust granular materials possessing complex geometries.

A key feature of the ink introduced here is its ability to vary the composition of 3D printed objects locally without risking the introduction of weak interfaces that would sacrifice their mechanical properties. This feature can be achieved if materials

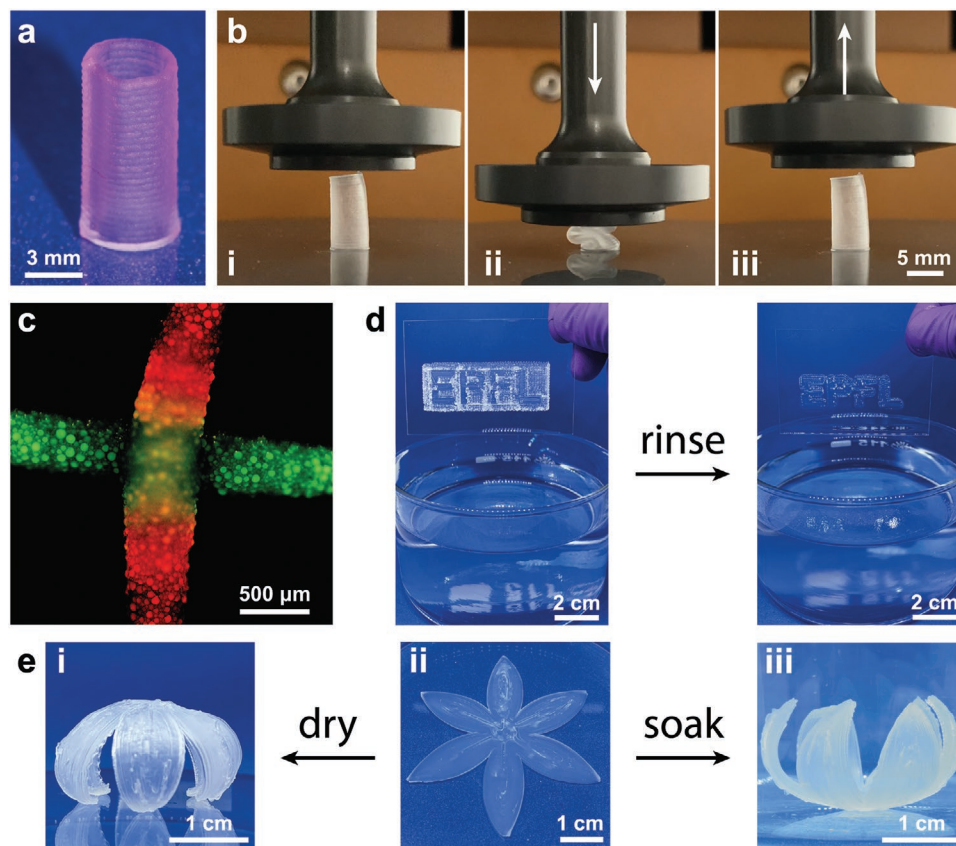


Figure 7. 3D printing of DNGHs. a) Photograph of a hollow cylinder with an aspect ratio of 2 that can be printed with high shape fidelity. Microgels are labeled with sulforhodamine B for better visualization. b) Photographs of the hollow DNGH cylinder under compression. While compressed, the cylinder experiences strong deformation and buckling. The good elasticity of DNGH allows the cylinder to return to its initial shape when the stress is released. c) Fluorescent micrograph of two filaments labeled with different dyes, demonstrating the ability to control the composition locally. d) Photographs of an object that has been 3D printed with a structural and sacrificial ink. The sacrificial ink can be removed after the secondary network of the structural ink has been formed by immersing the material into an aqueous solution. e) Photographs of dual-ink printing of a shape-morphing flower. The object is fabricated from two layers with different swelling behaviors. The first layer is composed of microgels containing 3.5 mol% cross-linker, the microgels contained in the second layer contain 14 mol% cross-linker. As a result of the different swelling behaviors of the microgels and the secondary network, that ensures a good integrity of the overall structure, the DNGH flower can repetitively fold in opposite directions upon drying and immersion in water.

are 3D printed from multiple inks, each one composed of jammed microgels possessing a well-defined composition that varies between the different inks; and all microgels are soaked in the same type of monomer solution. This ink formulation allows covalent crosslinking of adjacent microgels even if these microgels originate from different types of inks and hence possess different compositions after they have been processed into complex 3D structures. To demonstrate feasibility, we print an ink containing red microgels and one containing green microgels into a grid where the two types of hydrogels remain spatially separated, as illustrated in Figure 7c. To demonstrate the importance of the second percolating network for the mechanical stability of the DNGHs, we print the EPFL logo from a structural ink composed of microgels that are soaked in a monomer-containing solution and fill the interstices with a sacrificial ink, namely one composed of jammed microgels that do not contain any monomers. After the second percolating network is formed through exposure to UV-light, we selectively remove the sacrificial ink by immersing the 3D printed structure into an aqueous solution. We obtain an integral material possessing well-defined centimeter-sized structures, as illustrated in Figure 7d and Movie S4, Supporting Information.

To demonstrate the advantage of co-printing inks composed of microgels possessing different properties we 3D print shape-morphing DNGHs. Shape-morphing properties can be imparted to complex structures if they display anisotropic swelling behaviors.^[62–64] To obtain this property, we employ microgels with different crosslink densities such that their swelling behavior varies. Indeed, if we print a flower whose first layer is composed of microgels possessing a lower crosslink density than those contained in the second layer, the flower folds into opposite directions upon drying and soaking, as exemplified in Figure 7e. This example demonstrates the power and versatility of the presented method to fabricate responsive, smart, and soft materials that are sufficiently strong and stiff to bear significant loads.

3. Conclusion

We introduce a modular, versatile method to additive manufacture strong and tough complex hydrogels. The hydrogels are composed of jammed microgels that are connected through a second covalently cross-linked percolating network. Our approach combines the advantageous rheological properties of jammed microgels with the excellent mechanical properties of double network hydrogels to additive manufacture strong and tough granular hydrogels that can optionally be rendered adaptive. Because adjacent microgels are embedded in a percolating 3D network, the mechanical properties of the additive manufactured materials are isotropic and independent of the printing direction. Importantly, the two-step approach to fabricate DNGH is not limited to hydrogel particles but can be extended to a broad range of materials that can be processed into porous particles. Thereby, it significantly enlarges the range of materials that can be 3D printed into complex mechanically robust materials. The flexibility in the granular ink design and excellent control over the micrometer length scale structure opens up new possibilities to design the next generation of strong and

tough soft robots and implants that can adapt their properties locally in response to external stimuli.

4. Experimental Section

Materials: AMPS (Sigma-Aldrich, 282731), AM (Sigma-Aldrich, A4058), MBA (Carl Roth, 7867.1), 2-hydroxy-2-methylpropiophenone (PI) (Sigma-Aldrich, 405655), mineral oil light (Sigma-Aldrich, 330779), Span80 (TCI Chemicals, S0060), sulforhodamine B sodium salt (Sigma-Aldrich, S1402), fluorescein disodium salt (Carl Roth, 5283.1), and ethanol (Sigma-Aldrich, 459844) were all used as received.

Preparation of PAMPS Microgels: An aqueous solution containing 30 wt% AMPS, 3.5 mol% MBA, and 3.5 mol% PI was prepared, unless specified differently. The aqueous phase was emulsified with a mineral oil solution containing 2 wt% Span80. The water-in-oil emulsion was stirred while being illuminated with UV light (OmniCure S1000, Lumen Dynamics, 320–390 nm, 60 mW cm⁻²) for 5 min to convert drops into microgels. The resulting PAMPS microgels were transferred into ethanol and centrifuged at 4700 rpm for 15 min (Mega Star 1.6R, VWR) to remove the oil. The supernatant was discarded, and the process was repeated thrice with ethanol and thrice with water. Clean PAMPS microgels were resuspended in water for storage. To render microgels fluorescent, the authors added 0.05 mg of sulforhodamine B sodium salt or fluorescein disodium salt per milliliter of microgel solution.

Preparation of Jammed PAMPS ink: The solution containing dispersed PAMPS microgels was centrifuged and the supernatant was exchanged with excess aqueous solution containing 20 wt% AM, 0.2 mol% MBA, and 1.5 mol% PI. Microgels were soaked overnight. The solution containing PAMPS microgels was vacuum filtrated (Steriflip 50 mL tube, 0.22 μm, Millipore) to yield a jammed microgel ink.

Preparation of Molded DNGHs: The granular ink was casted into Teflon molds of cylindrical ($d = 8$ mm, $h = 2$ mm) or rectangular ($15 \times 5 \times 2$ mm³) shape, for compression and tensile measurements, respectively. The samples were cross-linked for 5 min under UV light (UVP CL-1000, Analytik Jena, 365 nm, 2 mW cm⁻²).

Preparation of Bulk Double Network Hydrogels: An aqueous solution containing 30 wt% AMPS, 3.5 mol% MBA, and 3.5 mol% PI was prepared. The AMPS solution was casted into Teflon molds for tensile measurements. The samples were cross-linked for 5 min under UV light (UVP CL-1000, Analytik Jena, 365 nm, 2 mW cm⁻²). PAMPS hydrogels were immersed overnight in an aqueous solution containing 20 wt% AM, 0.2 mol% MBA, and 1.5 mol% PI. Soaked samples were then exposed to UV illumination for 5 min to trigger the PAM second network percolation.

3D Printing of DNGHs: The jammed microgel ink was loaded in a 3 mL Luer lock syringe. To remove trapped air, the syringe was sealed and centrifuged at 4700 rpm for 1 min. Additive manufacturing of jammed microgels was performed with a commercial 3D bioprinter (Inkredible+, Cellink). The granular ink was extruded from a conical nozzle (410 μm) through a pressure driven piston (30 kPa). Printing was controlled through G-code commands that were generated by a built-in machine software (Cellink HeartWare). Printing was performed on a glass substrate with a starting gap of 0.1 mm. Printed structures were cross-linked by exposing them to UV light (UVP CL-1000, Analytik Jena, 365 nm, 2 mW cm⁻²) for 5 min.

Rheology of Jammed PAMPS Microgels: Rheology was performed on a DHR-3 TA Instrument with an 8 mm diameter parallel plate steel geometry. All measurements were performed at 25 °C, with an 800 μm gap. Frequency dependent viscosity measurements were made at 0.5% strain. Amplitude sweep was performed at 1.0 rad s⁻¹ oscillation. Self-healing measurements were performed at 1.0 rad s⁻¹, alternating 200 s at 1% strain, with 200 s at 30% strain. Samples were allowed to relax for 200 s at the set temperature before a measurement starts. Stress relaxation measurements were made for cross-linked and uncrosslinked microgels with an initial step strain of 10% and measured for 10 s. The gelation measurement was done at 1% strain and 10 rad s⁻¹ frequency

for 250 s. The liquid sample was loaded on the rheometer, and the UV lamp was switched on at $t = 25$ s to initiate the polymerization reaction.

Mechanical Characterization of DNGHs: Tensile measurements were performed with a commercial machine (zwickiLine 5 kN, 100 N load cell, Zwick Roell). Rectangular DNGH were mounted and stretched at a constant velocity of 100 mm min^{-1} . The Young's modulus was calculated as the slope of the initial linear region (from 5% to 15% strain). The toughness was calculated as the area below the stress-strain curve of an un-notched sample until fracture. The quantity was expressed as the energy absorbed until fracture per unit volume (J m^{-3}). Compression measurements were performed on a rheometer equipped with a parallel plate geometry (DHR-3, 50 N load cell, TA Instrument). Cylindrical DNGH were compressed at a constant velocity of 1.2 mm min^{-1} until 60% strain was reached.

Dry Polymer Content and EWC: The dry polymer content of AMPS microgels and DNGHs was calculated as the ratio of dry sample weight over as-prepared weight ($W_d/W_{ap} \cdot 100$). The EWC was calculated as the ratio of dry sample weight over fully swollen sample weight ($W_d/W_s \cdot 100$).

Supporting Information

Supporting Information is available from the Wiley Online Library or from the author.

Acknowledgements

M.H. and A.C. contributed equally to this work. The authors thank Mathias Steinacher and Huachuan Du for helpful and fruitful discussions. The work was financially supported by the Swiss National Science Foundation (SNSF, 200020_182662) and the Swiss National Competence in Research (NCCR) Bio-inspired Materials.

Conflict of Interest

We filed a patent on the ink formulation.

Keywords

3D printing, biomaterials, double networks, hydrogels

Received: July 14, 2020

Revised: September 28, 2020

Published online:

- [1] H. Yuk, C. E. Varela, C. S. Nabzdyk, X. Mao, R. F. Padera, E. T. Roche, X. Zhao, *Nature* **2019**, *575*, 169.
- [2] J. Li, D. J. Mooney, *Nat. Rev. Mater.* **2016**, *1*, 16071.
- [3] A. Ali, S. Ahmed, *J. Agric. Food Chem.* **2018**, *66*, 6940.
- [4] K. Y. Lee, D. J. Mooney, *Chem. Rev.* **2001**, *101*, 1869.
- [5] J. M. Lowen, J. K. Leach, *Adv. Funct. Mater.* **2020**, 1909089.
- [6] C. F. Guimarães, L. Gasperini, A. P. Marques, R. L. Reis, *Nat. Rev. Mater.* **2020**, *5*, 351.
- [7] C. Yang, Z. Suo, *Nat. Rev. Mater.* **2018**, *3*, 125.
- [8] X. Liu, J. Liu, S. Lin, X. Zhao, *Mater. Today* **2020**, *36*, 102.
- [9] Y. Lee, W. J. Song, J.-Y. Sun, *Mater. Today Phys.* **2020**, *15*, 100258.
- [10] D. E. Fullenkamp, L. He, D. G. Barrett, W. R. Burghardt, P. B. Messersmith, *Macromolecules* **2013**, *46*, 1167.
- [11] S. C. Grindy, M. Lenz, N. Holten-Andersen, *Macromolecules* **2016**, *49*, 8306.
- [12] A. Bin Imran, K. Esaki, H. Gotoh, T. Seki, K. Ito, Y. Sakai, Y. Takeoka, *Nat. Commun.* **2014**, *5*, 5124.
- [13] E. A. Appel, J. del Barrio, X. J. Loh, O. A. Scherman, *Chem. Soc. Rev.* **2012**, *41*, 6195.
- [14] D. Gan, W. Xing, L. Jiang, J. Fang, C. Zhao, F. Ren, L. Fang, K. Wang, X. Lu, *Nat. Commun.* **2019**, *10*, 1487.
- [15] Q. Li, D. G. Barrett, P. B. Messersmith, N. Holten-Andersen, *ACS Nano* **2016**, *10*, 1317.
- [16] L. Han, X. Lu, K. Liu, K. Wang, L. Fang, L.-T. Weng, H. Zhang, Y. Tang, F. Ren, C. Zhao, G. Sun, R. Liang, Z. Li, *ACS Nano* **2017**, *11*, 2561.
- [17] L. Han, X. Lu, M. Wang, D. Gan, W. Deng, K. Wang, L. Fang, K. Liu, C. W. Chan, Y. Tang, L.-T. Weng, H. Yuan, *Small* **2017**, *13*, 1601916.
- [18] Z. Tao, H. Fan, J. Huang, T. Sun, T. Kurokawa, J. P. Gong, *ACS Appl. Mater. Interfaces* **2019**, *11*, 37139.
- [19] J. P. Gong, Y. Katsuyama, T. Kurokawa, Y. Osada, *Adv. Mater.* **2003**, *15*, 1155.
- [20] T. Nonoyama, S. Wada, R. Kiyama, N. Kitamura, M. T. I. Mredha, X. Zhang, T. Kurokawa, T. Nakajima, Y. Takagi, K. Yasuda, J. P. Gong, *Adv. Mater.* **2016**, *28*, 6740.
- [21] J. P. Gong, *Science* **2014**, *344*, 161.
- [22] Z. Wang, *Soft Matter* **2019**, *15*, 3133.
- [23] W. M. Gramlich, I. L. Kim, J. A. Burdick, *Biomaterials* **2013**, *34*, 9803.
- [24] H. Lee, J.-H. Kim, G. Wu, H.-M. Lee, J. Kim, D. Kwon, S. Yang, C.-K. Kim, H. Yoon, *Adv. Mater. Interfaces* **2018**, *5*, 1801142.
- [25] W. Lei, S. Qi, Q. Rong, J. Huang, Y. Xu, R. Fang, K. Liu, L. Jiang, M. Liu, *Adv. Mater.* **2019**, *31*, 1808217.
- [26] J. M. McCracken, V. P. Tondiglia, A. D. Auguste, N. P. Godman, B. R. Donovan, B. N. Bagnall, H. E. Fowler, C. M. Baxter, V. Matavulj, J. D. Berrigan, T. J. White, *Adv. Funct. Mater.* **2019**, *29*, 1903761.
- [27] M. O. Saed, C. P. Ambulo, H. Kim, R. De, V. Raval, K. Searles, D. A. Siddiqui, J. M. O. Cue, M. C. Stefan, M. R. Shankar, T. H. Ware, *Adv. Funct. Mater.* **2019**, *29*, 1806412.
- [28] H. Zeng, D. Martella, P. Wasylczyk, G. Cerretti, J.-C. G. Lavocat, C.-H. Ho, C. Parmeggiani, D. S. Wiersma, *Adv. Mater.* **2014**, *26*, 2319.
- [29] E. C. Davidson, A. Kotikian, S. Li, J. Aizenberg, J. A. Lewis, *Adv. Mater.* **2020**, *32*, 1905682.
- [30] T. Priemel, E. Degtyar, M. N. Dean, M. J. Harrington, *Nat. Commun.* **2017**, *8*, 14539.
- [31] M. J. Harrington, F. Jehle, T. Priemel, *Biotechnol. J.* **2018**, *13*, 1800133.
- [32] H. Du, A. Cont, M. Steinacher, E. Amstad, *Langmuir* **2018**, *34*, 3459.
- [33] F. G. Downs, D. J. Lunn, M. J. Booth, J. B. Sauer, W. J. Ramsay, R. G. Klemperer, C. J. Hawker, H. Bayley, *Nat. Chem.* **2020**, *12*, 363.
- [34] J. E. Mealy, J. J. Chung, H.-H. Jeong, D. Issadore, D. Lee, P. Atluri, J. A. Burdick, *Adv. Mater.* **2018**, *30*, 1705912.
- [35] C. B. Highley, K. H. Song, A. C. Daly, J. A. Burdick, *Adv. Sci.* **2019**, *6*, 1801076.
- [36] A. Sheikhi, J. de Rutte, R. Haghniaz, O. Akouissi, A. Sohrabi, D. D. Carlo, A. Khademhosseini, *Biomaterials* **2019**, *192*, 560.
- [37] J. M. de Rutte, J. Koh, D. D. Carlo, *Adv. Funct. Mater.* **2019**, *29*, 1900071.
- [38] B. Kessel, M. Lee, A. Bonato, Y. Tinguely, E. Tosoratti, M. Zenobi-Wong, *Adv. Sci.* **2020**, *7*, 2001419.
- [39] S. Xin, D. Chimene, J. E. Garza, A. K. Gaharwar, D. L. Alge, *Biomater. Sci.* **2019**, *7*, 1179.
- [40] M. Shin, K. H. Song, J. C. Burrell, D. K. Cullen, J. A. Burdick, *Adv. Sci.* **2019**, *6*, 1901229.
- [41] A. Sheikhi, J. de Rutte, R. Haghniaz, O. Akouissi, A. Sohrabi, D. D. Carlo, A. Khademhosseini, *MethodsX* **2019**, *6*, 1747.
- [42] J. Saito, H. Furukawa, T. Kurokawa, R. Kuwabara, S. Kuroda, J. Hu, Y. Tanaka, J. P. Gong, N. Kitamura, K. Yasuda, *Polym. Chem.* **2011**, *2*, 575.
- [43] R. Takahashi, K. Shimano, H. Okazaki, T. Kurokawa, T. Nakajima, T. Nonoyama, D. R. King, J. P. Gong, *Adv. Mater. Interfaces* **2018**, *5*, 1801018.

- [44] D. Chimene, C. W. Peak, J. L. Gentry, J. K. Carrow, L. M. Cross, E. Mondragon, G. B. Cardoso, R. Kaunas, A. K. Gaharwar, *ACS Appl. Mater. Interfaces* **2018**, *10*, 9957.
- [45] D. Chimene, L. Miller, L. M. Cross, M. K. Jaiswal, I. Singh, A. K. Gaharwar, *ACS Appl. Mater. Interfaces* **2020**, *12*, 15976.
- [46] P. Menut, S. Seiffert, J. Sprakel, D. A. Weitz, *Soft Matter* **2011**, *8*, 156.
- [47] J. Hu, K. Hiwatashi, T. Kurokawa, S. M. Liang, Z. L. Wu, J. P. Gong, *Macromolecules* **2011**, *44*, 7775.
- [48] J. Hu, T. Kurokawa, T. Nakajima, T. L. Sun, T. Suekama, Z. L. Wu, S. M. Liang, J. P. Gong, *Macromolecules* **2012**, *45*, 9445.
- [49] E. Ducrot, Y. Chen, M. Bulters, R. P. Sijbesma, C. Creton, *Science* **2014**, *344*, 186.
- [50] S. Ding, B. Zou, P. Wang, H. Ding, *Polym. Test.* **2019**, *78*, 105948.
- [51] M. Liu, X. Zeng, C. Ma, H. Yi, Z. Ali, X. Mou, S. Li, Y. Deng, N. He, *Bone Res.* **2017**, *5*, 17014.
- [52] G.-L. Ying, N. Jiang, S. Maharjan, Y.-X. Yin, R.-R. Chai, X. Cao, J.-Z. Yang, A. K. Miri, S. Hassan, Y. S. Zhang, *Adv. Mater.* **2018**, *30*, 1805460.
- [53] Z. Chen, D. Zhao, B. Liu, G. Nian, X. Li, J. Yin, S. Qu, W. Yang, *Adv. Funct. Mater.* **2019**, *29*, 1900971.
- [54] W. Liu, O. Erol, D. H. Gracias, *ACS Appl. Mater. Interfaces* **2020**, *12*, 33267.
- [55] Y. Cheng, K. H. Chan, X.-Q. Wang, T. Ding, T. Li, X. Lu, G. W. Ho, *ACS Nano* **2019**, *13*, 13176.
- [56] F. Yang, V. Tadepalli, B. J. Wiley, *ACS Biomater. Sci. Eng.* **2017**, *3*, 863.
- [57] L. A. Hockaday, K. H. Kang, N. W. Colangelo, P. Y. C. Cheung, B. Duan, E. Malone, J. Wu, L. N. Girardi, L. J. Bonassar, H. Lipson, C. C. Chu, J. T. Butcher, *Biofabrication* **2012**, *4*, 035005.
- [58] J. Wei, J. Wang, S. Su, S. Wang, J. Qiu, Z. Zhang, G. Christopher, F. Ning, W. Cong, *RSC Adv.* **2015**, *5*, 81324.
- [59] S. Hong, D. Sycks, H. F. Chan, S. Lin, G. P. Lopez, F. Guilak, K. W. Leong, X. Zhao, *Adv. Mater.* **2015**, *27*, 4035.
- [60] E. A. Guzzi, G. Bovone, M. W. Tibbitt, *Small* **2019**, *15*, 1905421.
- [61] B. Zhang, S. Li, H. Hingorani, A. Serjouei, L. Larush, A. A. Pawar, W. H. Goh, A. H. Sakhaei, M. Hashimoto, K. Kowsari, S. Magdassi, Q. Ge, *J. Mater. Chem. B* **2018**, *6*, 3246.
- [62] A. S. Gladman, E. A. Matsumoto, R. G. Nuzzo, L. Mahadevan, J. A. Lewis, *Nat. Mater.* **2016**, *15*, 413.
- [63] O. Erol, A. Pantula, W. Liu, D. H. Gracias, *Adv. Mater. Technol.* **2019**, *4*, 1900043.
- [64] Y. Kim, H. Yuk, R. Zhao, S. A. Chester, X. Zhao, *Nature* **2018**, *558*, 274.